Tau-induced mitochondrial membrane perturbation is dependent upon cardiolipin

Angelique Camilleri[a], Stephanie Ghio[a], Mario Caruana[a], Daniel Weckbecker[b], Felix Schmidt[c], Frits Kamp[d], Andrei Leonov[b,e], Sergey Ryazanov[e], Christian Griesinger[e], Armin Giese[c], Ruben J. Cauchi[a], Neville Vassallo[a,*]

[a] *Department of Physiology and Biochemistry, Centre for Molecular Medicine and Biobanking, University of Malta, Msida, Malta*
[b] *MODAG GmbH, Wendelsheim, Germany*
[c] *Center for Neuropathology and Prion Research, Ludwig-Maximilians-University, Munich, Germany*
[d] *Biomedical Center-BMC, Metabolic Biochemistry, Ludwig-Maximilians-University, Munich, Germany*
[e] *Department of NMR Based Structural Biology, Max Planck Institute for Biophysical Chemistry, Göttingen, Germany*

ARTICLE INFO

ABSTRACT

Misfolding and aggregate formation by the tau protein has been closely related with neurotoxicity in a large group of human neurodegenerative disorders, which includes Alzheimer's disease. Here, we investigate the membrane-active properties of tau oligomers on mitochondrial membranes, using minimalist *in vitro* model systems. Thus, exposure of isolated mitochondria to oligomeric tau evoked a disruption of mitochondrial membrane integrity, as evidenced by a combination of organelle swelling, efflux of cytochrome *c* and loss of the mitochondrial membrane potential. Tau-induced mitochondrial dysfunction occurred independently of the mitochondrial permeability transition (mPT) pore complex. Notably, mitochondria were rescued by pre-incubation with 10-N-nonyl acridine orange (NAO), a molecule that specifically binds cardiolipin (CL), the signature phospholipid of mitochondrial membranes. Additionally, NAO prevented direct binding of tau oligomers to isolated mitochondria. At the same time, tau proteins exhibited high affinity to CL-enriched membranes, whilst permeabilisation of lipid vesicles also strongly correlated with CL content. Intriguingly, using single-channel electrophysiology, we could demonstrate the formation of non-selective ion-conducting tau nanopores exhibiting multilevel conductances in mito-mimetic bilayers. Taken together, the data presented here advances a scenario in which toxic cytosolic entities of tau protein would target mitochondrial organelles by associating with their CL-rich membrane domains, leading to membrane poration and compromised mitochondrial structural integrity.

1. Introduction

Tau is considered to be the most frequently misfolded protein linked to human neurodegenerative disease, with deposition of abnormal tau in the brain being a defining feature of more than 20 disorders. These include Alzheimer's disease (AD), frontotemporal lobar degeneration (FTD), progressive supranuclear palsy, corticobasal degeneration, Pick's disease and others [1]. The most prevalent tauopathy is AD; it represents the main cause of dementia among older adults, and is characterised clinically by a progressive decline in cognitive abilities [2]. The classic neuropathological hallmark of AD is the co-existence of extracellular plaques consisting of aggregates of the amyloid-beta (Aβ) peptide and intraneuronal fibrillary tangles (NFTs) composed mainly of the tau protein [3]. Although for over 20 years amyloid plaques were regarded as the central event that triggered AD, current thought is that the propagation of tau pathology correlates better with synaptic loss and progression to the clinical (symptomatic) stage of AD [4]. Thus, therapeutic strategies aimed at antagonising misfolded tau and

compensating for the loss of normal tau function have now emerged [5,6].

Tau is a microtubule-associated protein abundantly expressed in the central nervous system (CNS) and has key roles in regulating axonal transport and maintaining neuronal integrity. Tau proteins are expressed from six different isoforms generated by alternative splicing of a primary transcript harbouring 16 exons. Hence, full-length tau protein varies between 352 and 441 amino acid residues in length, with molecular weights (based on amino acid composition) of 36–46 kDa depending on the tau isoform. The longest isoform (2N4R) contains two acidic inserts at the N-terminal and all four microtubule-binding regions at the C-terminal [7]. Two hexapeptide repeats in R2 and R3 have a strong tendency to aggregate and form the rigid β-rich core region of paired helical filaments (PHFs), the major constituents of NFTs [8,9]. Tau aggregation is promoted by numerous factors, including missense and deletion mutations, high local protein concentration, hyperphosphorylation by brain kinases, polyanionic factors, and the presence of metal ions like iron or aluminium [10–12]. Although tau is abnormally phosphorylated at multiple positions in AD, it has been shown that non-phosphorylated tau is able to support tau aggregation intracellularly [13,14].

Considerable researches postulate that the major neurotoxic tau species are the soluble aggregates that precede formation of the larger fibrillar NFT deposits [15–17]. Most recently, an *in vivo* two-photon imaging study in mice expressing both human Aβ and tau revealed a potent suppression of neural circuits which was dependent specifically on soluble tau [18]. Tau toxicity most likely originates from the dimers, trimers and other low-molecular-weight species [19]. In particular, direct injection of recombinant tau oligomers, but not monomers or fibrils, caused memory impairments, synaptic dysfunction and mitochondrial damage when applied intracerebrally to wild-type mice [20]. Conversely, removal of tau oligomers in an AD mouse model was associated with improved morphology of neuronal dendritic spines and ameliorated memory deficits [21]. Further, tau oligomers were significantly elevated in human brains in cases of progressive supranuclear palsy and AD, where they appeared in early pre-tangle neurons [22].

The easy accessibility of cellular and organelle membranes to cytosolic tau have made the study of tau-lipid bilayer interactions of great relevance to understanding disease pathology, with several studies having implicated membranes as important targets for oligomeric tau aggregates [23]. When artificial phospholipid vesicles were treated with tau monomers, oligomers or fibrils, the most effective increase in membrane leakage was induced by the oligomeric species [15]. Association of free tau with anionic synthetic particles and anionic lipid vesicles seeded aggregation of tau and disruption of lipid packing within the membrane, while neutral zwitterionic bilayers remained intact [24–26]. Tau-induced membrane permeabilisation was hypothesised to result from the alignment of tau multimers into pore-like structures [27]. Mitochondrial membranes are obvious targets for toxic intracellular tau species, not least in synapses where mitochondria are especially abundant [28]. Subcortical injection of recombinant tau oligomers into brains of mice provoked mitochondrial dysfunction, by decreasing complex I activity and activation of the apoptotic mitochondrial pathway leading to synaptic dysfunction [20,29]. In transgenic mice with mutant P301L tau overexpression, functional analysis confirmed mitochondrial dysfunction in the form of reduced mitochondrial respiration and ATP synthesis [30]. Other reports have demonstrated a direct role for tau in altering mitochondrial trafficking, distribution and dynamics [31–33].

The signature phospholipid of mitochondrial membranes is cardiolipin (1,3-diphosphatidyl-*sn*-glycerol, CL) which accounts for ~10% of the total mitochondrial phospholipids [34]. Mitochondrial contact sites, which represent regions of close apposition between the outer mitochondrial membrane (OMM) and inner mitochondrial membrane (IMM), are particularly enriched in CL (~25%) [34]. CL has a diphosphatidylglycerol backbone combined with four acyl chains,

resulting in a dimeric arrangement and a conical structure which is unique among phospholipids [35]. CL is fundamental for mitochondrial bioenergetics and participates in the organisation of the respiratory components of the electron transport chain into supercomplexes for optimal oxidative phosphorylation [36]. CL is also an essential component of a mitochondrial signalling platform for the activation of apoptosis, with the oxidative state of CL influencing mobilisation of cytochrome *c* (cyt *c*) from the mitochondria [37,38].

In previous work, we had established the permeabilising abilities of oligomer aggregates of full-length tau-441 in lipid vesicles with defined membrane compositions [39]. Particularly intriguing was the finding that mitochondrial membranes appeared to be especially vulnerable to aggregate insult. In the present study, we sought to deduce further insight into the destabilisation of mitochondrial membranes by amyloidogenic tau, focusing especially on a possible role for CL in mediating tau interaction with mitochondria. To this end, we employed model systems consisting of isolated reconstituted membranes with complex lipid compositions mirroring the biophysical properties of the mitochondrial bilayer.

2. Materials and methods

2.1. Tau protein handling and aggregation

Recombinant human tau protein (hTau46, 1N4R isoform) was expressed from a pRK172 vector in BL21(DE3) *E. coli* cells and purified as described previously [40]. Tau stock solutions (1 mg/ml) were stored frozen in 50 mM Tris-Cl (pH 7.0) at −80 °C in LoBind microfuge tubes (Eppendorf). To avoid repeated freeze/thaw cycles and hence pre-aggregation of the protein, stocks were divided into aliquots and were regularly checked by gel electrophoresis (Supplementary Fig. S1). Only samples free of pre-formed aggregates were used. Tau was aggregated using published protocols: 7 μM monomeric tau was incubated in 70 μM AlCl$_3$ and DPBS without agitation at 37 °C for 96 h [11]. This protocol generates an oligomer-rich tau preparation, which was confirmed using a combination of gel electrophoresis, bis-ANS dye to detect surface hydrophobicity characteristic of oligomers, and fluorescence spectroscopy analysis at the single-particle level (Supplementary Fig. S1). Aggregated tau was frozen in liquid nitrogen and stored at −80 °C. The protein was thawed to room temperature (RT) directly before use in downstream assays.

2.2. Isolation of mitochondria from SH-SY5Y cells

Mitochondria were isolated from SH-SY5Y human neuroblastoma cells (purchased directly from ECACC UK, Cat #94030304) using a MITOISO2 kit (Sigma-Aldrich, Germany) essentially as previously described, to yield an enriched mitochondrial fraction with viable, intact mitochondria [39]. The mitochondrial pellet was resuspended in 1× mitochondrial buffer (MB: 10 mM HEPES, 5 mM succinate, 250 mM sucrose, 1 mM ATP, 0.08 mM ADP, 2 mM K$_2$HPO$_4$, 1 mM DTT, pH 7.5) at 1–2 mg/ml. Mitochondria were kept on ice during the entire isolation procedure and prepared fresh for each experiment. The purity of the mitochondrial fraction was confirmed by immunoblot analysis of cytosolic and mitochondrial isolates with anti-Hsp90 monoclonal (Abcam Cat #13492) and anti-cyt *c* monoclonal (Thermo Fisher Scientific Cat #456100) primary antibodies (Supplementary Fig. S2).

2.3. Mitochondrial swelling assay

Freshly isolated mitochondria (100 μg total mitochondrial protein) were brought to an initial A$_{540}$ of ~0.35–0.4 in 1 × MB and swelling was initiated by adding 500 μM CaCl$_2$, tau, or other swelling agent. When required, mitochondria were pre-treated with compounds for 10 min. 4,4′-diisothiocyanostilbene-2,2′-disulfonic acid (DIDS), cyclosporin A (CsA) were purchased from Sigma-Aldrich (Munich, Germany).

Bongkrecic acid (BKA) and anti-VDAC rabbit polyclonal antibody (Cat #AP1059) were from Calbiochem (Darmstadt, Germany). Readings of A_{540} were taken from duplicate samples, every 5 min for 60 min at RT. After subtracting the blank (buffer alone) from all values, data was expressed as means of absorbance readings ± SEM.

2.4. Measurement of the membrane potential of isolated mitochondria

Isolated mitochondria (5 μg total mitochondrial protein) were stained with the JC-1 kit (Isolated Mitochondria Staining Kit, Sigma-Aldrich, Germany) for measurement of the mitochondrial membrane potential ($\Delta\psi_m$) according to kit instructions. JC-1 fluorescence was monitored at RT for 30 min, using 490 nm excitation and 590 nm emission in a microplate reader (FLX800, Bio-Tek, Germany). Samples were tested in triplicate and the $\Delta\psi_m$ obtained by subtracting the average FCCP (carbonyl cyanide-p-trifluoromethoxyphenylhydrazone) baseline, representing complete dissipation of the $\Delta\psi_m$, from the maximal JC-1 fluorescence measured.

2.5. Immunoblotting for cytochrome c release

Isolated mitochondria (20 μg total mitochondrial protein) were incubated with the indicated concentrations of tau for 60 min at RT in 1 × MB. Reaction mixtures were centrifuged at 16,000g for 10 min at 4 °C to pellet mitochondria, and cyt *c* release detected by probing the resultant supernatant with anti-cyt *c* monoclonal antibody (Thermo Fisher Scientific Cat #456100). Briefly, equal aliquots of the supernatant were subjected to NuPAGE gel electrophoresis using 4–16% Bis-Tris gels (Life Technologies) and transferred to Hybond-ECL membrane (Amersham, GE Healthcare). After blocking overnight at 4 °C and washing three times in TBS-T buffer (Tris-buffered saline, 0.05% Tween-20), the blot was probed with primary anti-cytochrome *c* antibody (1:1000 in TBS-T) for 1 h with gentle shaking. After washing, the membrane was then exposed to the horseradish peroxidase-conjugated anti-mouse secondary antibody (1:4000 in TBS-T) followed by chemiluminescence detection using ECL Prime kit (Amersham, GE Healthcare). A semi-quantitative assessment of the intensity of cyt *c* bands was carried out using scans and software (ImageJ Software, NIH Image).

2.6. Dot blot analysis for tau binding to isolated mitochondria

Freshly isolated mitochondria (25 μg total mitochondrial protein) were incubated for 15 min at 37 °C in the presence of 7 μM oligomeric tau. When needed, mitochondria were pre-incubated for 10 min with 20 μM NAO prior to adding tau. Unbound tau was removed by centrifugation at 12,000g for 30 min at 4 °C. Mitochondrial pellets were washed twice with DPBS and the final mitochondrial pellet lysed in CelLytic™ M containing Protease Inhibitor Cocktail (MITOISO2 kit; Sigma-Aldrich, Germany) and subjected to dot blot analysis on nitrocellulose membranes. Membrane strips were blocked in 10% non-fat dry milk in TBS-T for 1 h at RT with agitation, washed and probed with mouse monoclonal Tau-5 antibody (Abcam Cat #ab3931) (1:3000 in 5% non-fat dry milk in TBS-T) for 1 h at RT under agitation. Following multiple washes (5 min in wash buffer, 4–6×) the membranes were incubated with anti-mouse secondary antibody (1:12,000 in TBS-T) for another 1 h at RT under agitation. Chemiluminescent detection was carried out using ECL Prime kit (Amersham, GE Healthcare).

2.7. NAO (10-N-nonyl acridine orange)-cardiolipin binding assay

In this assay, formation of NAO dimers induced by binding to CL in solution results in a decrease in the absorbance of NAO at 495 nm and appearance of a maximum at 474 nm [41]. All experiments were done in deionised water to optimise electrostatic interactions of tau peptides with phospholipids. The solvent used to dissolve the phospholipids

(chloroform) had negligible effect on the absorbance spectra. Phospholipids (CL or PC), with or without tau aggregates, were pipetted into 96-well clear half-area plate (Costar) and the plate was left for 20 min at RT, with shaking every 5 min. Next, NAO (0.5 μM, final concentration) was added to sample wells and absorbance readings at 495 nm and 474 nm taken in quadruplicate using an absorbance reader (BMG Lab-tech Spectrostar Nano). The average absorbance reading of the blank control was subtracted from all values, and the data expressed as A495/A474 ratio.

2.8. Liposome preparation and membrane permeability assay

The phospholipids L-α-phosphatidylcholine (egg PC), L-α-phosphatidylethanolamine (egg PE), L-α-phosphatidylinositol (soy PI), L-α-phosphatidylserine (brain PS), DOPE:DOPS:DOPC (5:3:2 w/w/w) and heart cardiolipin (CL) were purchased from Avanti Polar Lipids, Inc. (Alabaster, AL, USA). Phospholipids dissolved in chloroform were handled using a glass Hamilton syringe and always kept on ice. Unilamellar liposomes, loaded with the Ca^{2+}-binding indicator Oregon Green 488 BAPTA-1 (OG) (Invitrogen) for the leakage assays, were prepared using the detergent-dialysis method as previously described [39]. The lipid ratios (% by weight of total phospholipids) are based on published data on the lipid compositions of the OMM, IMM and contact sites [34,42]. *IM-type* (mimics IMM and mitochondrial contact sites): 45% PC, 25% PE, 10% PI, 5% PS and 15% CL; *OM-type* (mimics OMM): 52% PC, 27% PE, 9% PI, 7% PS and 5% CL; *L-type* (same as IMM composition but lacks CL): 60% PC, 25% PE, 10% PI and 5% PS. For the gel retardation assay, an additional *C-type* (mimics synaptic vesicle membrane) was used consisting of 50% DOPE, 30% DOPS, 20% DOPC (*w/w/w*). Vesicles were suspended in liposome buffer (100 mM KCl, 10 mM MOPS/Tris, 1 mM EDTA, pH 7.0) and stored at 4 °C. Liposome sizing was performed by dynamic light scattering (DLS) measurements using a Zetasizer Nano-ZS (Malvern Instruments, UK). Each sample was analysed in triplicate in clear disposable cells. On average, liposomes were found to have a diameter of ~120 nm, hence classified as large unilamellar vesicles (LUVs).

For the liposome permeabilisation assays, 25 μM OG-loaded LUVs in liposome buffer containing 0.1 mM CaCl$_2$ were exposed to 0.1 μM pre-aggregated tau species. An increase in fluorescence yield due to OG-calcium binding implied loss of membrane integrity. Measurements (in triplicate) were performed in black 96-well plates (Costar) at RT for 60 min, using a fluorescence microplate reader (FLx800-TBID, Bio-Tek, Germany) with an excitation wavelength of 485 nm and emission wavelength of 528 nm. The maximum fluorescence intensity ($F_{max} = 100\%$) was determined by the addition of the calcium ionophore ionomycin (2 μM). The percentage permeabilisation value was calculated according to the equation:

$$Permeabilisation\ (\%) = 100 \times (F - F_0)/(F_{max} - F_0)$$

where F denotes the maximum fluorescence intensity of the measured sample over 60 min, and F_0 represents the fluorescence of intact vesicles.

2.9. Phospholipid-tau native blue gel retardation assay

A native gel retardation (or shift binding) assay is useful to demonstrate direct protein binding to lipid vesicles [43]. Oligomeric tau (1.4 μM) was incubated in liposome buffer (100 mM KCl, 10 mM MOPS/Tris, pH 7.0) with LUVs containing 0% (C-type) and 15% (IM-type) cardiolipin in their membrane composition, for 15 min at RT. The protein-lipid samples were then subjected to NativePAGE in 4–16% Bis-Tris gels (Invitrogen) and stained with GelCode Blue (Thermo Fisher Scientific, USA).
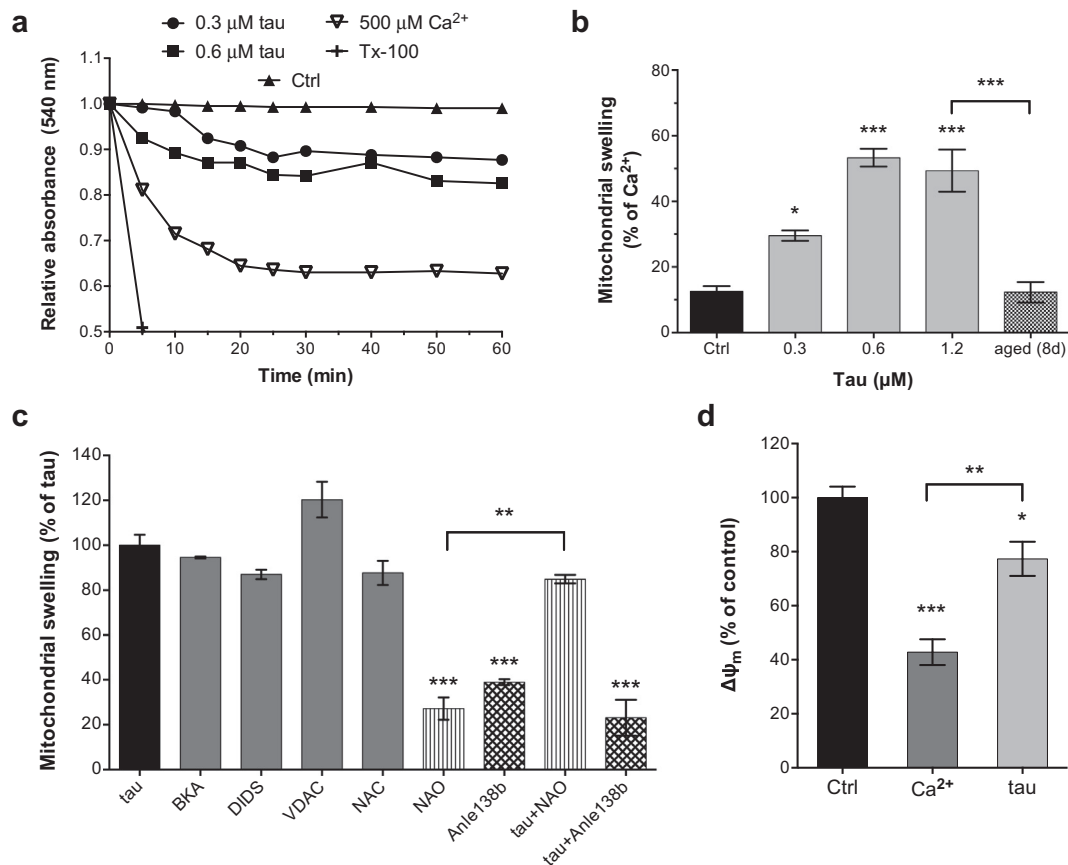
Fig. 1. Tau oligomer-induced mitochondrial swelling and inhibition of $\Delta\psi_m$. (a–c) Mitochondrial swelling induced by tau oligomers is independent of mPT and inhibited by NAO. (a) Assay showing changes in absorbance at 540 nm due to mitochondrial swelling upon addition of exogenous oligomeric tau; the membrane detergent Triton X-100 (TX; 0.5% v/v) caused immediate mitochondrial lysis. Ctrl represents mitochondria in tau aggregation buffer only. The swelling assays were performed in five independent experiments, and a representative tracing is shown. (b) Mitochondrial swelling was monitored for 60 min, and maximal swelling by tau was calculated as a percentage of that induced by 500 μM Ca^{2+} alone. Oligomeric (4-day aggregated) tau was compared with aged tau (8-day aggregated) at 1.2 μM (in equivalent moles of monomer). Values are the means $\pm$ SEM of five independent experiments ($n = 5$) with duplicate sample measurements. (c) Prior to the initiation of swelling by addition of oligomeric tau (0.6 μM), the mitochondrial suspension was pre-incubated for 10 min with: inhibitors of the mPT pore complex which act on the IMM (BKA, 10 μM) or the OMM (DIDS, 50 μM and anti-VDAC antibody, 1 μg/ml), the thiol antioxidant NAC (5 mM), the CL-binding molecule NAO (20 μM), and the anti-aggregator compound anle138b (10 μM). NAO and anle138b were also tested by incubating these compounds with tau oligomers for 20 min before adding the compound-oligomer mixture to the mitochondrial suspension (tau + NAO and tau + anle138b, respectively). Swelling in the presence of each compound is given as a percentage of tau alone (100%). The results shown are the means $\pm$ SEM of three independent experiments ($n = 3$) with triplicate sample measurements. (d) Oligomeric tau aggregates (1.2 μM) or Ca^{2+} ions (500 μM) were incubated with mitochondria and $\Delta\psi_m$ determined using the JC-1 probe. $\Delta\psi_m$ is given as a percentage of untreated mitochondria control (100%), with baseline obtained by dissipating $\Delta\psi_m$ using FCCP. Data are presented as means $\pm$ SEM of three independent experiments ($n = 3$) with triplicate sample measurements. ***$p < 0.005$, **$p < 0.01$, and *$p < 0.05$, relative to control or between marked pairs (one-way ANOVA plus Bonferroni post-test).

2.10. Electrophysiological setup and measurements

Electrophysiological studies were performed using the Ionovation Compact workstation (Ionovation GmbH, Osnabrück, Germany) on an isolated vibration-free table [44]. A dried lipid mixture (typically, IM-type) was dissolved in n-decane (purity > 99%) and 1.5 μl applied onto the pinhole separating the *cis* and *trans* chambers using the painting technique [45], until a BLM was formed. Bilayer formation was monitored visually using a dedicated camera and by capacitance measurements. Bilayers typically had a capacitance between 50 and 70 pF and background conductances of < 15 pS. Membranes that showed instability, abnormal capacitance, or abnormal conductance were discarded and replaced.

After at least 15 min of a stable bilayer system, pre-aggregated tau peptide (0.4 μM, in equivalent moles of monomeric tau) was applied into the buffer solution directly below the bilayer in the *cis* compartment. For the compound-added trials, the aggregated tau/anle138b mixture was preincubated for 90 min prior to addition to the bilayer chamber. Initially, miniature magnetic bars stirred the solutions on

both sides of the membrane to facilitate insertion of protein into the BLM. Buffer conditions were symmetrical with 250 mM KCl, 10 mM MOPS/Tris (pH 7.2) in both *cis-trans* compartments. In the event of an increase in bilayer conductance (> 70 pS) and a pore event, currents in response to varying applied voltages were recorded using standard protocols automatically run by Patchmaster software (HEKA, Germany): (i) voltage-ramping from −60 mV to +60 mV over 10 s, and vice-versa; (ii) square wave-voltage pulses of −60, −50, −40, −30, −20, −10, 0, +10, +20, +30, +40, +50, +60 mV, with 10 s recording at each voltage; (iii) 100 s runs of recordings at ± 40 mV potential, repeated for three times. Ion selectivity was determined by changing to an asymmetrical salt concentration (250:20 mM KCl, *cis:trans*) to enable measurement of the reversal potential. An electrophysiology experimental trial typically lasted ~2 h. Current recordings were analysed using the Clampfit 10 software package (Molecular Devices). Further statistical analysis was done using GraphPad Prism 6 (GraphPad Software, Inc.).

2.11. Estimation of pore diameter

The pore diameter was estimated from defined conductance levels assuming a simplified cylindrical nanopore, hence conductance G is directly proportional to the pore cross-sectional area. Under this assumption, the pore diameter ($2r$) can be calculated by the following equations [46]:

$$r = r_0[1 + (1 + 4L/\pi r_0)^{1/2}] \qquad (1)$$

$$r_0 = G/4\sigma \qquad (2)$$

where r is the pore radius, G the single pore conductance, L the pore length, and σ the bulk electrolyte solution conductivity (measured as 29.1 mS/cm at 25 °C for 250 mM KCl). We assumed l to be equal to the membrane thickness, i.e. 7 nm for mitochondrial membranes [47].

2.12. Statistical analysis

All statistical analyses, graphs and curve fitting were conducted using GraphPad Prism (version 6; GraphPad Software Inc., La Jolla, USA). Mean and standard error of the mean (SEM) was used to present the results, with n as the number of independent experiments. The number of sample replicates within each experiment is given for each data set. Differences between means for more than two groups were determined by one-way analysis of variance (ANOVA) with a post-hoc Bonferroni correction for false positives. Data were tested for normality using D'Agostino-Pearson test. Densitometric analysis of immunoblots was performed on the uncompressed original gray-scale depth TIFF image files without image enhancement, and the normalised intensity values were averaged to represent the mean and standard deviation (SD) of all of the determinations performed. In all analyses, a value of $p < 0.05$ was considered to be significant; exact p values are given whenever possible.

3. Results

3.1. Tau-induced swelling and cytochrome c release from isolated mitochondria are inhibited by the cardiolipin-specific dye NAO

We carried out three different assays to investigate perturbation of mitochondrial membrane integrity by physiologically-relevant (μM) concentrations of pre-aggregated tau oligomers: the mitochondrial swelling assay, cyt c efflux and measurement of the inner mitochondrial membrane potential ($\Delta\psi_m$). Swelling kinetics were monitored upon incubation of isolated mitochondria with 0.3–0.6 μM oligomeric tau, with Ca^{2+} ions included as a positive control [48]. Significant swelling started after around 10 min incubation with 0.3 μM tau, while exposure to 0.6 μM tau increased mitochondrial volume in less than 5 min (Fig. 1A). When tau-induced swelling was calculated as a percentage of that triggered by Ca^{2+} ions alone, a dose-dependent effect on swelling was noted from 0.3 μM (29 $\pm$ 2%, $p = 0.03$) to 0.6 μM (53 $\pm$ 3%, $p < 0.0001$) tau, when compared to untreated mitochondria. Notably, treatment with 1.2 μM aged (8-day aggregated) tau did not significantly increase swelling (12 $\pm$ 3%, $p > 0.05$), unlike the pronounced swelling effect of 1.2 μM oligomeric (4-day aggregated) tau (49 $\pm$ 6%, $p < 0.0001$) (Fig. 1B). Taken together, swelling data are in agreement with the notion that soluble tau oligomers, but not protofibrillar tau species, can be highly damaging to mitochondrial membranes.
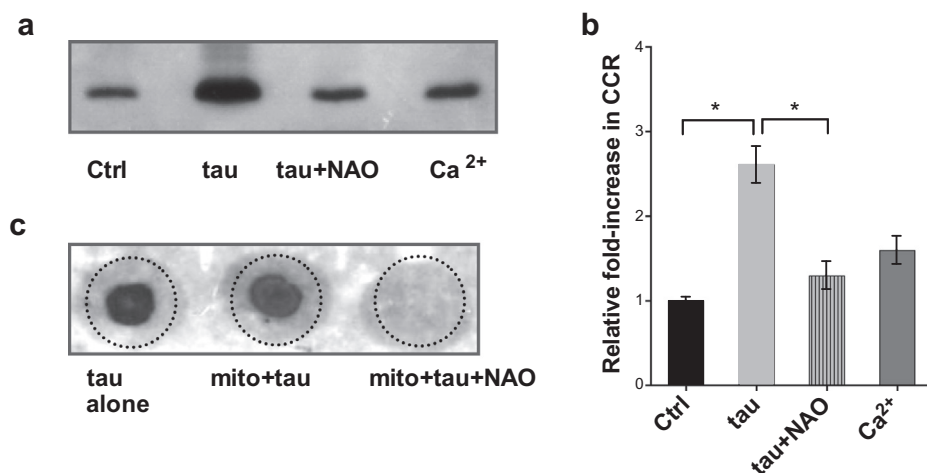
Tau-induced swelling might involve formation and opening of the mitochondrial permeability transition (mPT) pore complex in isolated mitochondria [49]. Hence, we attempted suppression of tau-induced swelling by pre-incubating the mitochondria with inhibitors of essential outer and inner membrane components of the mPT pore, specifically: inhibitors of the voltage-dependent anion channel (VDAC) component in the OMM (DIDS and anti-VDAC antibody) and of the adenine nucleotide translocator (ANT) component in the IMM (BKA) [50,51]. The

powerful thiol antioxidant N-acetyl-cysteine (NAC) was also tested, given the possible involvement of reactive oxygen species (ROS) in triggering mPT formation. However, none of these mPTP pore modulators had any significant inhibitory effect on swelling, implying an mPT-independent mechanism and pointing to a direct consequence of tau interaction with mitochondrial membranes (Fig. 1C). When mitochondria were pre-incubated with the fluoroprobe 10-N-nonyl acridine orange (20 μM NAO), however, a marked inhibition of mitochondrial swelling was observed (27 $\pm$ 5% swelling, $p < 0.0001$) (Fig. 1C). Given that NAO is highly specific to binding the phospholipid CL (and hence the IMM or contact sites) [52], the inference from this experiment was that CL might play a role in the directed targeting of tau oligomers to mitochondrial membranes. The NAO effect was dose-dependent, since a lower concentration of 10 μM NAO inhibited tau-induced swelling to 64 $\pm$ 6% of tau alone ($n = 3$; $p < 0.01$), while a higher concentration of 40 μM NAO was significantly toxic to mitochondria, and actually increased mitochondrial swelling to 140% of tau alone ($n = 3$; $p < 0.001$) (data not shown). The latter can be readily explained from previous reports that NAO at high concentrations could disturb mitochondrial membrane structure and bioenergetic functioning [53].

We additionally tested the novel oligomer modulator anle138b [3-(1,3-benzodioxol-5-yl)-5-(3-bromophenyl)-1H-pyrazole] in the swelling assay. Anle138b is a diphenylpyrazole compound that was reported to inhibit tau aggregation in $vitro$ and delay disease progression in a transgenic mouse model (PS19) of tauopathy [40]. Here, anle138b effectively decreased organelle swelling induced by tau (39 $\pm$ 2% swelling, $p < 0.0001$), thus also confirming the involvement of tau oligomers in membrane permeabilisation (Fig. 1C). Finally, we wanted to verify that the observed effect with NAO was due to interaction of NAO with mitochondrial membranes, rather than with the protein oligomers. Hence, the swelling experiment was repeated following a 20-min pre-incubation of NAO or anle138b with the tau oligomers. This experimental strategy allowed the compounds to interact extensively with, and possibly bind to, the aggregated tau species prior to mitochondrial exposure. While this strategy lead to an enhanced inhibitory effect on tau-induced swelling of the anti-oligomer anle138b compound (23 $\pm$ 8% swelling, $p < 0.0001$ $vs.$ tau alone), the protective effect of NAO was on the other hand abrogated (85 $\pm$ 2% swelling, $p > 0.05$ $vs.$ tau alone) (Fig. 1C). The inference is that, in keeping with its key physicochemical property as a CL-binding probe, the potent inhibitory effect shown by NAO against tau-induced mitochondrial swelling is indeed a consequence of its interaction with the mitochondrial membrane, and not the tau protein oligomers.

In the same assay setting, we investigated the impact of tau on the $\Delta\psi_m$ of isolated mitochondria (Fig. 1D). Over a 30 min exposure to oligomeric tau, the $\Delta\psi_m$ was significantly decreased compared to control (78 $\pm$ 6%, $p = 0.0249$). Depolarisation of the $\Delta\psi_m$ was also observed with 500 μM Ca^{2+} ions (43 $\pm$ 5%, $p = 0.0003$), which again acted as a positive control. Unlike in the swelling assays, we could not investigate the effect of NAO on the tau-induced drop in $\Delta\psi_m$ due to the high intrinsic fluorescence of NAO.

Swelling of the mitochondrial organelle often leads to rupture of the OMM and depletion of cyt c from the intermembrane spaces – a critical event in the conduction of downstream apoptotic pathways in cells [54]. Therefore, we sought to investigate whether, when incubated with isolated mitochondria under the same conditions as for the swelling assay, oligomeric tau is able to evoke significant cyt c release (CCR) and whether NAO can mitigate this process. Indeed, densitometric analysis of immunoblots carried out for the detection of released cyt c from mitochondria exposed to exogenous tau, confirmed a robust 2.6-fold increase in CCR compared to mitochondria alone ($p = 0.0129$; Fig. 2A and B). Modest CCR was also imparted by addition of Ca^{2+} ions (1.6-fold increase), used as a positive control. Most importantly, pre-incubation of the mitochondria with NAO significantly prevented tau-induced CCR (1.3-fold increase, $p = 0.0273$ $vs.$ tau alone) (Fig. 2B).

Fig. 2. Release of cyt *c* from isolated mitochondria by oligomeric tau is inhibited by NAO. (a and b) Mitochondria were exposed to oligomeric tau alone (0.6 μM tau), pre-incubated with the CL-specific probe NAO before addition of tau (tau + NAO), or incubated with 500 μM Ca^{2+} ions as a positive control (Ca^{2+}). Ctrl represents untreated mitochondria. Visualisation of CCR was done by probing the supernatant with anti-cytochrome *c* antibody. The blot is representative of three independent experiments ($n = 3$). Full-length immunoblot is presented in Supplementary Fig. S5. For densitometric analysis, bars represent the average normalised intensity of the two replicate experiments, shown as fold-increase in CCR compared to Ctrl (untreated mitochondria). (c) Dot blots showing interference by NAO with tau binding to mitochondria. Binding of pre-aggregated tau to isolated mitochondria in the absence (mito + tau) and presence of NAO (mito + tau + NAO) was visualised by dot blot analysis probed with Tau-5 antibody. Mitochondria were pre-incubated for 10 min with 20 μM NAO before addition of tau. Recombinant tau (1 μg) without mitochondria was included as a control for the dot blot procedure (tau alone). Representative dot blot is shown, with similar results obtained in two additional independent experiments.

These data further indicate that CL might be playing an important targeting role when exposing isolated mitochondria to soluble tau aggregates.

3.2. NAO interferes with binding of tau to isolated mitochondria

A direct interpretation of the swelling and CCR experiments was that soluble tau aggregates were causing mitochondrial damage through the presence of CL in the membranes. In order to examine further this hypothesis, we looked at the direct binding of tau with mitochondria. Thus, freshly isolated mitochondria were left to incubate with pre-aggregated tau for 15 min, and the mitochondrial pellet probed in dot blots for the presence of tau particles (Fig. 2C). Strikingly, when mitochondria were pre-incubated with NAO, the tau blot signal was however completely absent (Fig. 2C). We concluded that the addition of NAO, as a selective CL-binding probe, was competitively preventing binding of tau to mitochondria, hence corroborating the role of the mitochondrial phospholipid CL in targeting of tau to mitochondria. Additional control experiments using recombinant tau alone excluded the possibility that NAO might be directly interfering, in a non-specific manner, with tau binding to the nitrocellulose membrane and/ or with chemiluminescence from the tau-secondary HRP antibody complex (Supplementary Fig. S3). Moreover, NAO had no influence on tau aggregation or the formation of tau oligomers (Supplementary Fig. S4).

3.3. Studies of tau and NAO binding to free cardiolipin

We next considered whether the tau aggregates would be able to compete with NAO for binding to free CL molecules in solution. Selective binding of NAO molecules to CL phospholipids causes a decrease in the absorbance of the monomeric form at 495 nm. Additionally, a maximum appears at 474 nm, resulting in an absorbance ratio (495 nm/474 nm) of less than 1.0 [41]. In fact, the OD 495/474 ratio fell to well below 1.0 when NAO was combined with 4 μM CL (0.68 ± 0.07, $p < 0.0001$ *vs.* NAO alone), but not with PC (1.49 ± 0.02, $p > 0.05$ *vs.* NAO alone) or PS (1.29 ± 0.05, $p > 0.05$ *vs.* NAO alone). This confirmed specificity of NAO binding to the CL phospholipid, as reported in many studies [53,55] (Fig. 3). There was also no significant change in the OD 495/474 ratio when 2 μM CL was pre-incubated with either 2 μM (0.91 ± 0.02) or even 20 μM (0.98 ± 0.0) aggregated tau before addition of NAO, compared to CL alone (0.84 ± 0.1). This implies that tau oligomers could not
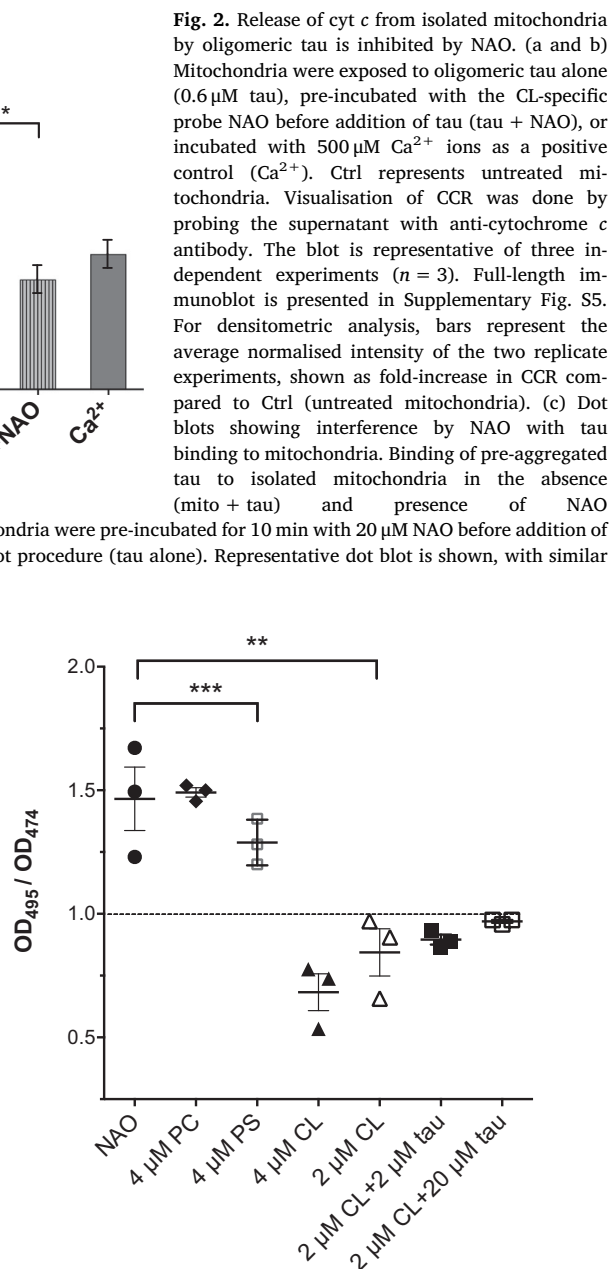

Fig. 3. Studies of tau-cardiolipin interactions by absorption spectra. The NAO-CL competitive binding assay was used to investigate possible tau-CL interactions in solution. An absorbance ratio (495 nm/474 nm) of less than 1.0 indicates NAO binding to CL, as a result of depletion of free NAO molecules. Exposure of CL to oligomeric tau, before adding NAO, did not significantly increase the ratio to > 1.0. Absorbance readings were taken in quadruplicate. Scatter plots show means ± SEM ($n = 3$ independent experiments); ***$p < 0.0005$, **$p < 0.01$, between indicated pairs (one-way ANOVA plus Bonferroni post-test).

competitively prevent binding of CL with NAO.

3.4. Membrane cardiolipin content correlates with lipid vesicle permeabilisation and binding

To further support a correlation between mitochondrial membrane destabilisation by tau oligomers and CL content, dye leakage was tracked from lipid vesicles with membranes harbouring 0% (L-type), 5% (OM-type), and 15% (IM-type) CL. As illustrated in Fig. 4A, the 3 different lipid compositions were associated with a significantly
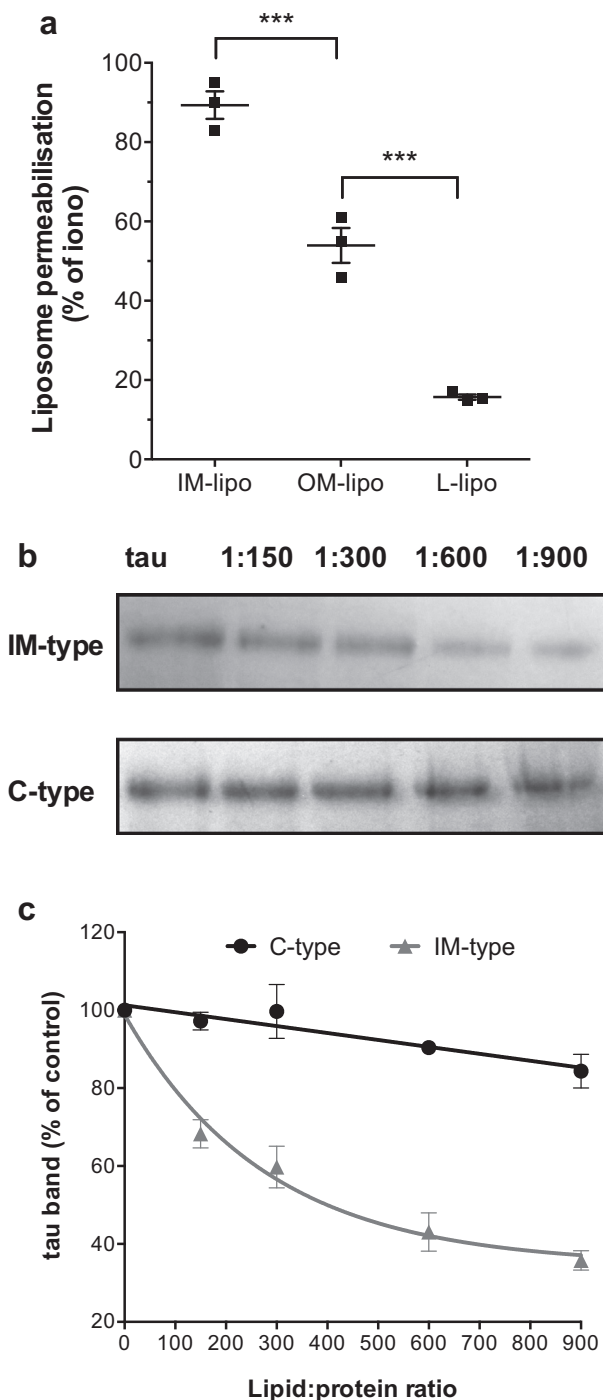
Fig. 4. (a) Liposome permeabilisation by tau correlates with CL content. Pre-aggregated oligomeric tau (0.1 μM) was incubated with three types of fluorophore-loaded LUVs: IM-type (15% CL, resembling the IMM and mitochondrial contact sites), OM-type (5% CL, resembling the OMM), and L-type (0% CL, as IM-type but completely lacking CL). Data is presented as percentage of the permeabilisation effect achieved by adding the calcium ionophore ionomycin (theoretical max, 100%). Values represent means ± SEM, each experiment performed using triplicate sample readings (n = 3 independent experiments); ***$p \le 0.005$, between marked pairs (one-way ANOVA plus Bonferroni post-test). (b) Gel retardation assay for binding of tau to LUVs. Oligomeric tau was incubated with IM-type (15% CL, 30% anionic) or C-type liposomes (0% CL, 30% anionic) at the indicated protein:lipid molar ratios and subjected to blue native PAGE. Tau bands are displayed (b) from a representative experiment. Full-length gel is presented in Supplementary Information Fig. S6. Densitometric analysis (c) shows % tau in the gel with increasing tau:lipid ratios (1:150–1:900). The data was fitted into an exponential decay function using GraphPad Prism. The curve-fitting (IM-type: R^2 = 0.9884; C-type: R^2 = 0.9000)

allowed calculation of the K_D value as an index of relative affinity of tau to IM-type (K_D = 124) and C-type (K_D = 937) membranes. Values represent means ± SEM (n = 4).

different extent of leakage; more specifically, a trend is apparent in which permeabilisation of IM-type (89%; p = 0.0008 vs. OM-type) > OM-type (53%; p = 0.005 vs. L-type) > L-type (16%) liposomes. In other words, a positive and robust correlation between the CL content of vesicle membrane and the extent of permeabilisation is indicated (Spearman rank-order correlation coefficient r = 0.9614, 95% CI) with the greatest affinity of oligomeric tau being for IM-type (15% CL) membranes.

To follow up on this finding, a native gel retardation assay was used to examine the effect of CL content on the binding of tau protein to large unilamellar vesicles (LUVs). With this aim, two types of LUVs were utilised: IM-type vesicles with membranes having 15% CL, and C-type vesicles with membranes that lack CL completely and which model synaptic vesicle membranes [56]. Importantly, C-type membranes have the same overall negative charge density (30% anionic) as IM-type membranes, thereby allowing us to control for an effect of anionic charge on tau binding. Using the gel retardation assay, we found that tau indeed interacts more favourably with CL-containing LUV membranes, as clearly shown by the steady decline in the intensity of the tau band with increasing lipid:protein ratios for IM-type, but not C-type, vesicles (Fig. 4B). Densitometric band analysis indicated that at the highest lipid:protein (900:1) ratio tested, the presence of tau protein in the gel decreased substantially to ~35% of control (tau alone) due to binding with IM-type LUVs, compared with a decrease to only ~84% in the presence of C-type LUVs (Fig. 4C). Calculation of the equilibrium dissociation constant (K_D) for IM-type and C-type membranes by non-linear regression analysis yielded values of K_D = 124 and K_D = 937, respectively. Hence, tau exhibited a ~7.5-fold higher affinity to CL-enriched membranes. In conclusion, the gel retardation assay supported the notion that tau directly binds CL liposomes more avidly than liposomes having multicomponent CL-deficient lipid membranes, irrespective of the overall negative charge of the bilayer.

3.5. Single-channel electrophysiology of tau pores in mito-mimetic membranes

Having found that oligomeric tau is highly membrane-active in both the isolated mitochondria and liposomal models, it was interesting to address the possibility of formation of ion-conducting pores in mito-mimetic membranes by tau protein complexes. Evidence for pore formation in biologically-relevant membrane compositions was sought using the technique of single-channel electrophysiology. The standard approach in single-channel electrophysiology involves protein reconstitution into a freestanding bilayer lipid membrane (BLM) separating two electrolyte solutions, followed by application of a transmembrane electric field and a detailed electrophysiological evaluation of the recorded currents [45]. Electrophysiological characterisation allows identification of channel conductances, determination of I-V relationships, analysis of ion selectivity and estimation of pore size.

It was first determined that addition of the oligomer-enriched tau preparation to the cis-chamber with applied voltages of ± 40 mV resulted in the appearance of a highly-reproducible "flickering" ion channel-like activity, as represented by the fast, transient, step-wise transitions visible in the current traces, typically after a delay of around 20 min (20 ± 12 min, n = 8 trials) (Fig. 5A). On the other hand, control experiments without any protein showed no changes in membrane conductance over 120 min (n = 8 trials). Tau incorporation was recorded in 45% of trials (n = 9/20 trials) when using the cardiolipin-containing IM-type membrane for the electrophysiology bilayer. To look at a possible influence of CL on the membrane incorporation events, a comparison was made with L-type and C-type bilayers. Indeed,
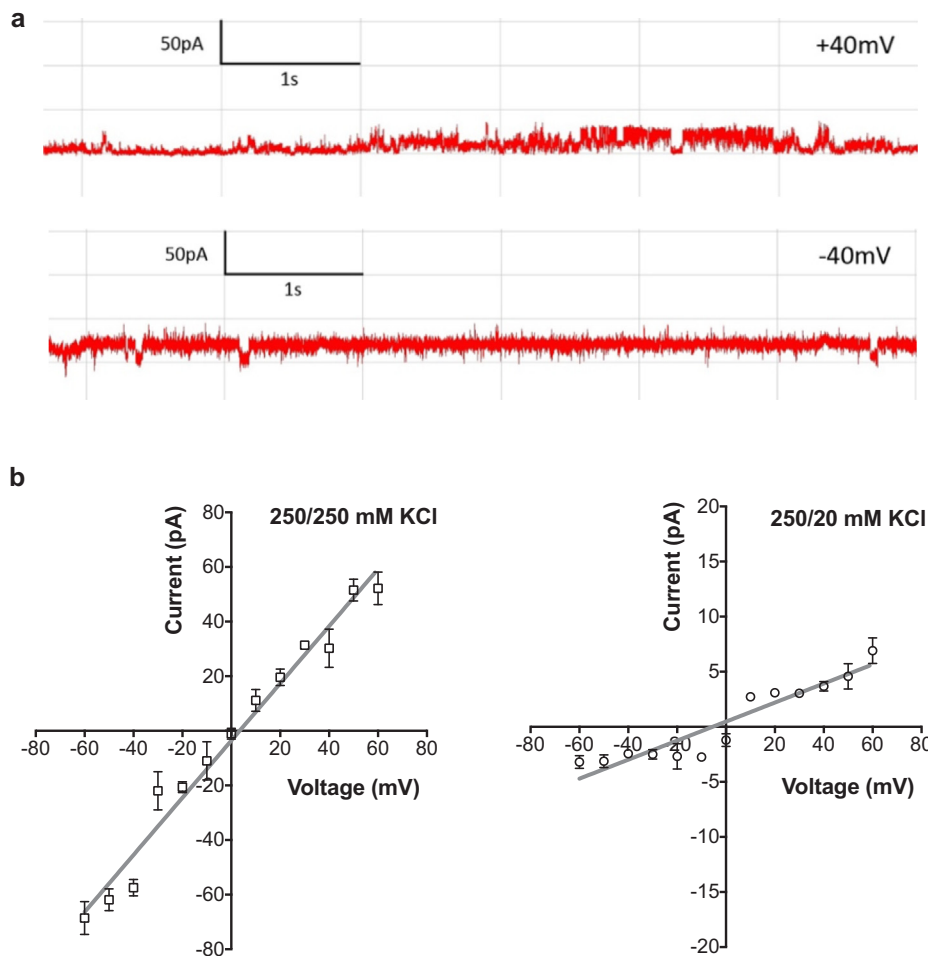
a

b

Fig. 5. (a) Sample traces showing channel-like activity with frequent spikes of ionic current after addition of oligomeric tau (400 nM) to the *cis*-side of the chamber at the indicated voltage-clamp conditions. Current flow was measured across the IM-type BLM in 250 mM KCl buffer (in both chambers). The induced currents are indicative of the formation of tau nanopores in the BLM. (b) Current-voltage relationship for a single tau pore in IM-type lipid bilayer. *Left panel* Current measurements during voltage ramping from −60 mV to +60 mV under symmetrical buffer conditions (250/250 mM KCl, 10 mM MOPS/Tris, pH 7.2). The *I-V* data set is fitted with a linear regression. Error bars represent standard deviation. ($n = 2$ independent experiments). *Right panel* Current-voltage ramp under asymmetrical buffer conditions (250/20 mM KCl, 10 mM MOPS/Tris, pH 7.2). The intercept on the voltage axis equivalent to the reversal potential (E_{rev}) is at − 5 mV.

only 5% of trials with the L-type bilayer ($n = 1/20$ trials) and 10% of trials with the C-type bilayer ($n = 2/20$ trials) resulted in observation of channel-like currents over 2 h. Hence, in line with the previous liposome experiments, tau channel-like membrane activity was established most readily in membranes harbouring CL. Unfortunately, we could not test for an inhibitory effect of NAO on the channel-like activity of tau oligomers, since within 5–10 min of adding low micromolar concentrations (5–10 μM) of NAO to the buffer in the bilayer chamber, a high membrane conductance resulted which therefore precluded any further addition of tau oligomers.

Next, the current traces obtained when using IM-type BLMs were analysed for multi-level conductance behaviour that would identify formation of ion-conducting tau nanopores. Using Clampfit software, the conductance levels and conductance steps obtained from recorded traces at +40 mV applied voltage (a higher number of conductance steps were recorded at this voltage) were quantified and their distribution plotted in histograms. The Gaussian fits of the conductance level histogram (Fig. 6A) revealed a clear distribution of the conductivity, with distinct peaks at three consecutive conductance levels: ~340 pS (342 ± 42 pS; defined as *Open 1*), ~720 pS (717 ± 32 pS; defined as *Open 2*) and ~1200 pS (1195 ± 106 pS; defined as *Open 3*). Therefore, starting from 0 pS (closed state), the peak conductances identified above differ by steps of 340 pS (closed ↔ *Open 1*), 380 pS (*Open 1* ↔ *Open 2*) and 480 pS (*Open 2* ↔ *Open 3*). To complement the conductance levels histogram, a histogram of the conductance step sizes at +40 mV was also constructed. It showed a major peak at around 300–350 pS and no significant step size events beyond ~500 pS (Fig. 6B). Therefore, the data from the histogram of the step sizes was in agreement with that from the conductance levels histogram. Such well-

defined conductance levels with fixed step sizes would essentially conform to the formation of transmembrane pore complexes by tau, allowing permeability to ions across the BLM. Pore diameters for the three basic conductance levels were also calculated, by assuming a simplified cylindrical hole for a pore: *Open 1*, 1.1 nm; *Open 2*, 1.6 nm; *Open 3*, 2.1 nm [46].

Having obtained evidence for the formation of active pores by oligomeric tau in IM-type BLM, we proceeded to investigate possible voltage-dependence and ion selectivity characteristics by carrying out current-voltage ramp experiments on inserted pores. Under symmetric conditions (250/250 mM KCl), a linear *I-V* relationship was observed, meaning that the permeation rate through the pore was not being changed by, and hence was independent of, the membrane voltage (Fig. 5B). Furthermore, under asymmetric conditions (250/20 mM KCl) there was only a slight shift, from 0 mV to −5 mV, of the point at which the *I-V* curve cut the *x*-axis (known as the reversal potential E_{rev}). This indicates little ion selectivity of the pore between positively and negatively charged ions (Fig. 5B).

Anle138b was then tested to assess whether the small-molecule compound, which had effectively reduced mitochondrial swelling, could also decrease tau-induced ionic conductivity in IM-type BLM. Pore formation was monitored after the pre-aggregated tau had undergone prior incubation with anle138b. Out of six trials (hence a total of 12 h of monitoring for current activity across the BLM) not a single pore insertion event was detected ($n = 0/6$ trials). Thus, anle138b resulted in a complete abrogation of pore formation in IM-type lipid bilayers by tau aggregates. On the other hand, tau pore insertion and activity could not be prevented by adding 1 mM Zn^{2+} ions ($n = 3/6$ trials).
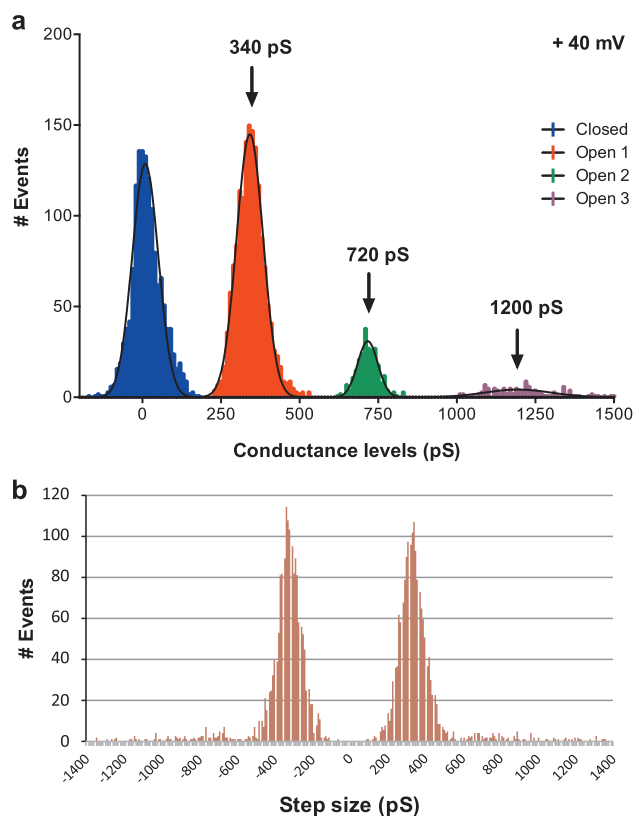
Fig. 6. Histograms of conductance levels and steps for tau pores recorded in IM-type bilayers. (a) Histogram analysis of all the open and close conductance states (*n* = 3,349 analysed events) at +40 mV applied holding potential from a typical single-channel recording of a detected pore. Data fitted to a Gaussian distribution (sold black lines) assigns peaks at ~350 pS (*Open 1*), ~700 pS (*Open 2*), and ~1100 pS (*Open 3*) indicted by arrows. (b) Histogram analysis of the corresponding step sizes from the same recording. Collectively, data shows a quantised distribution of conductance with a basic event of ~350–400 pS.

4. Discussion

Herein, we aimed to deduce new mechanistic insights into the consequences of mitochondrial exposure to exogenous tau oligomers. Our collective observations advance a model in which tau oligomeric aggregates associate directly with mitochondrial membranes to inflict mitochondrial dysfunction, with a decisive role being played by CL, a phospholipid abundant in mitochondrial contact sites and the IMM.

When isolated mitochondria were exposed to low micromolar concentrations of oligomeric tau, a combination of significant organelle swelling, major efflux of cyt *c* from mitochondria, and lowering of the $\Delta\psi_m$ were observed. Mitochondria from 8-month-old triple transgenic AD mice (combining both amyloid-β and tau pathologies) showed a similar (~20%) reduction of the $\Delta\psi_m$, with a further decrease in $\Delta\psi_m$ at 12 months [57]. In cellular studies, overexpression of human wild-type tau induced mitophagy deficits concomitant with tau protein accumulation in the OMM fraction [58]. In agreement, we also confirmed that the tau oligomers were bound to, and could be pelleted with, the mitochondria. One can therefore envisage direct interaction of tau with mitochondria, leading to swelling of the mitochondrial matrix and consequent rupture of the OMM, thereby allowing a portion of the cyt *c* to escape from the intermembrane space of mitochondria such that a decrease in the $\Delta\psi_m$ occurs. In addition, our electrophysiology data raise the possibility of amyloid tau pore or channel formation in mitochondrial membranes. The conductance level histograms clearly illustrate that current fluctuations are not random, but can be grouped into discrete multi-level conductance states. It is thus unlikely that the tau aggregates are interacting with the vertical BLM via the so-called 'carpet' mechanism, as previously reported for prefibrillar states of the islet amyloid polypeptide and some antimicrobial peptides [59,60]. Carpeting refers to accumulation of oligomeric assemblies at the membrane surface without penetration of the bilayer, hence inducing a lowering of the dielectric barrier and a non-specific generalised increase in conductance [61]. Rather, the electrophysiology recordings are consistent with a mechanism involving the reconstitution of oligomeric (characteristically β-sheet) subunits in the fluidic bilayer to create a range of protein-stabilised pores. This is in line with prior reports of channel formation by other amyloid-forming proteins, including amyloid-β, α-synuclein, islet amyloid polypeptide (IAPP) and others [62,63]. As is typical of active channels formed by amyloidogenic proteins, the ion permeation rate through the tau pores was not altered by changing the voltage across the bilayer [63]. Moreover, tau pores had estimated openings of 1–2 nm and exhibited no clear selectivity between negatively or positively charged ions. Such properties would be expected to allow uncontrolled passage of water, monovalent/divalent ions and small molecules through the nanopores and across mitochondrial membranes.

Since no structural information on the tau nanopores formed in the BLM was obtained in this study, their exact physical nature remains to be determined. Nonetheless, a combined analysis of the conductance level and step size histograms suggests that the observed multilevel channel conductances could reflect a different number of subunits making up a single pore, with sequential transitions from one main conductance level to another involving the addition, or removal, of an aggregate subunit to an inserted tau pore complex. In a recent study describing channel formation by oligomeric amyloid-β (1–42) peptides, the amyloid-β channels were large in size (hundreds of pS with pore diameters of 1.7–2.4 nm), voltage-independent and transiently flickered between multiple conductance states, mirroring the situation of our mitochondrial tau nanopores [64]. Electrophysiological characterisation of tau channels has to date only been attempted in one other study [65]. Tau channels were reported to be relatively nonselective and not responsive to zinc ions, as in the present investigation. On the other hand, described conductances were much lower (< 200 pS) and channel formation was seen only at an acidic pH of 5.2, with no activity recorded at pH 7.4 [65]. These differences can be accounted for by the fact that, in contrast to our electrophysiology studies, the authors made use of monomeric tau and simplified POPE:POPG (2:1) bilayers. Low pH is known to enhance tau binding affinity to anionic membranes and aggregation [25], thus possibly explaining why tau channels were only formed under these conditions.

Perhaps the most intriguing observations in our experiments relate to CL, the signature phospholipid of mitochondria. Our findings suggest that, by associating first with CL on mitochondrial membranes, the cardiolipin-specific dye NAO effectively blocked tau binding to isolated mitochondria and consequently protected against swelling and CCR. The assumption that NAO is specific for CL is based on extensive literature [41,53,66], and was confirmed here in the CL-NAO binding absorbance experiments. It is thought that the hydrophobic interaction between NAO and CL plays a more important role than electrostatic interaction, and that the selectivity might result from the insertion of the nonyl groups in the bilayer at the hydrophobic surface generate by the presence of four chains in the CL molecule [67,68]. The importance of CL for tau membrane activity was further reflected in the liposome permeabilisation assays, with an increasing CL membrane fraction correlating with increased vesicle disruption. The enhanced vulnerability of CL-rich membranes to permeation was also evident in the electrophysiology experiments: tau pore formation in planar bilayers was highest for the mito-mimetic (IM-type) BLM, and was markedly less when CL was excluded from the membrane composition. Moreover, increasing the lipid:protein ratio in the gel retardation assay manifestly increased binding of tau only to CL-containing lipid vesicles. Importantly, the preferential binding of tau oligomers to CL-containing membranes is potentially due to an affinity for the presence of the

phospholipid (i.e. CL) itself, rather than being primarily dependent on the negative surface charge of the bilayer imparted by CL. This was shown by use of the C-type (synaptic vesicle) membrane which, despite possessing the same overall negative charge density (30% anionic) as the IM-type membrane, was less susceptible to tau interaction and nanopore formation. It was previously reported that misfolded whole-length tau, or even tau repeat segments alone, associate with anionic phospholipid membranes, invoking structural transformations that could play a role in aggregation and membrane disruption [26,69]. Oligomeric tau intermediates were found to be the most toxic tau species, effectively decreasing cell viability and increasing phospholipid vesicle leakage [15]. Indeed, it is possible that anle138b protected against organelle swelling, and prevented formation of conducting tau pores on bilayers, by converting membrane-active tau oligomers into a membrane-inert state. In this regards, in another study it was proposed that anle138b triggered a conformational change in amyloid-β pores that turned them into a non-conductive state [70].

The observed affinity of tau aggregates to CL-containing membranes may thus result from a direct binding of oligomeric tau with CL at biomembrane surfaces in situ, which may be influenced by factors such as spontaneous curvature and packing defects of membranes with a high CL content. With its unique quadruple-chained structure and two negatively-charged phosphodiester moieties on its head group, CL significantly alters the physical properties of lipid membranes [71]. Generally speaking, the structure of CL confers a less compact environment between head groups and induces lipid packing defects in the mitochondrial membrane because of mismatch between the curvature of the bilayer and the cone shape of the lipid acyl chains [72,73]. In mitochondria, CL is particularly enriched at OMM contact sites (up to 24% CL content). Contact sites represent specialised domains where the outer and inner membranes are in close apposition, thus allowing CL to diffuse from the IMM to the OMM. CL microdomains tend to localise to regions of high intrinsic negative curvature, and are in fact hypothesised to control mitochondrial inner membrane organisation [74]. Not unexpectedly therefore, these localised, phase-segregated domains in mitochondria enriched in CL are believed to play a pivotal role in energy flux processes [75]. For instance, CL physically participates in the stabilisation of higher order supercomplexes comprised of respiratory complexes I, III, and IV in mammalian cells. Organisation of respiratory chain components into one structural and functional unit (referred to as a 'respirasome') greatly facilitates electron flux through the respiratory chain [76]. Additionally, CL functionally interacts with and forms proteolipid complexes in the IMM with mitochondrial creatine kinase and AAC, a major ADP/ATP carrier protein [77,78]. Such interactions permit the exchange of metabolites between the mitochondrial matrix and the cytosol, thus controlling mitochondrial respiration. Therefore, physical interaction of tau oligomers with CL and disruption of mitochondrial membrane phospholipids is likely to lead to a feed-forward loop of increased ROS production, inefficient oxidative phosphorylation and bioenergetic deficit. Evidence that a fraction of tau localises to mitochondria and is found at the OMM and within the intermembrane space, has recently emerged [79,80]. We plan further investigations focused on how tau affects various parameters of mitochondrial metabolism, including oxygen consumption, redox state and ATP production.

It is also worth commenting on the remarkable resemblance of our proposed mechanism of mitochondrial poration by tau with pro-apoptotic activity of members of the Bcl-2 family, such as Bax, Bak and Bid. For instance, oligomeric Bax pore formation requires mitochondria-specific CL, with 7% CL in the membrane being sufficient for Bax-induced mitochondrial permeabilisation [38]. Bax and Bak insert within curvature-induced lipid packing defects created by CL, leading to mitochondrial outer membrane permeabilisation and triggering of apoptosis [81,82]. Similarly, cytosolic truncated Bid (tBid) triggers CCR by preferentially associating with CL at mitochondrial contact sites and inducing a reorganisation of cristae [83,84]. What is more, in a striking

parallel with our observations, NAO inhibited CCR by blocking tBid binding to mitochondrial contact sites [85]. Through this mechanism, NAO protected myocardium against ischaemia-reperfusion injury in rats [52].

In future work, we plan to genetically manipulate the CL content in neuronal cells [43] and determine what effect this would have on mitochondrial susceptibility to tau aggregate insult. Presumably, lowering CL content should help protect against mitochondrial damage. In this way, we also directly address one of the main limitations of this work, namely that implication of the role of CL in mitochondrial targeting by tau depends to a large extent on the use, and specificity, of the dye NAO. Although NAO, a lipophilic cation, stains mitochondria selectively, it has been reported to bind anionic lipids like PI or PS at lower affinities [86,87]. Hence, a genetic approach might provide even stronger evidence that CL in the mitochondrial membrane is indeed critical for tau aggregate binding and toxicity to mitochondria. Another limitation of the current study is to what extent isolated mitochondria and artificial liposomes recapitulate cellular and biomembrane complexity. For instance, when expressed in cell lines (as opposed to briefly incubated with mitochondria in vitro as here), there may be greater opportunity for tau to exert its effects, so that subtle alterations of mitochondrial function can accumulate chronically. It would therefore be important to further investigate such aspects using cellular models.

Finally, our work may open up another new direction of study in the emerging field of membrane-targeting antibiotics [88]. Bacterial membranes have a significantly higher population of negative intrinsic curvature lipids than mammalian membranes, and it was shown that these differences can be exploited by anti-microbial peptides to differentially kill bacteria over mammalian cells [89]. Recently a new synthetic antibiotic, the cyclic hexapetide cyclo(RRRWFW), has been shown to target CL and cause redistribution of membrane lipids into different domains [90]. It is tempting to speculate whether aggregated amyloid-like proteins, including tau, Aβ and alpha-synuclein, can also kill bacteria with CL-rich membranes by pore formation.

5. Conclusion

In conclusion, our findings add significantly to an expanding body of research suggesting that CL-rich mitochondrial membranes, such as the outer membrane contact sites or the inner membrane, play an essential and active role in targeting of mitochondria by pore-forming protein assemblies. In the cytosol, toxic amyloid entities of tau protein would be free to engage with mitochondria by directly associating with CL or by inserting into lipid defects created by the CL molecules, leading to compromised mitochondrial function. An important therapeutic implication is that drug design to target CL may offer potential for restoring mitochondrial bioenergetics. A direct example is the Szeto-Schiller (SS) peptide SS-31, a first-in-class CL protective compound currently undergoing clinical trials which interacts selectively with CL to enhance mitochondrial respiration and ATP production [91,92]. Hence, efforts directed at developing drugs that target mitochondrial lipids, and especially CL, may constitute a new strategy for pharmacological therapy of neurodegenerative proteinopathies.

Declaration of Competing Interest

Acknowledgements

Author Contributions

N.V., R.J.C., A.G., A.C. and S.G. conceived and designed the experiments; A.C., S.G., M.C., and D.W. performed the experiments; N.V., A.G., S.G., and A.C., analysed the data; F.S., F.K., A.L., S.R. and C.G. contributed reagents/materials/analysis tools; N.V., A.C. and S.G. wrote the paper.

Appendix A. Supplementary material

Supplementary data to this article can be found online at https://doi.org/10.1016/j.bbamem.2019.183064.

References

[1] T. Arendt, J.T. Stieler, M. Holzer, Tau and tauopathies, Brain Res. Bull. 126 (2016) 238–292.

[2] P. Scheltens, K. Blennow, M.M. Breteler, B. de Strooper, G.B. Frisoni, S. Salloway, W.M. Van der Flier, Alzheimer's disease, Lancet 388 (2016) 505–517.

[3] A.W.P. Fitzpatrick, B. Falcon, S. He, A.G. Murzin, G. Murshudov, H.J. Garringer, R.A. Crowther, B. Ghetti, M. Goedert, S.H.W. Scheres, Cryo-EM structures of tau filaments from Alzheimer's disease, Nature 547 (2017) 185–190.

[4] M.J. Pontecorvo, M.D. Devous Sr., M. Navitsky, M. Lu, S. Salloway, F.W. Schaerf, D. Jennings, A.K. Arora, A. McGeehan, N.C. Lim, H. Xiong, A.D. Joshi, A. Siderowf, M.A. Mintun, F.A.-A. Investigators, Relationships between flortaucipir PET tau binding and amyloid burden, clinical diagnosis, age and cognition, Brain 140 (2017) 748–763.

[5] B. Bulic, M. Pickhardt, E. Mandelkow, Progress and developments in tau aggregation inhibitors for Alzheimer disease, J. Med. Chem. 56 (2013) 4135–4155.

[6] Y.L. Gao, N. Wang, F.R. Sun, X.P. Cao, W. Zhang, J.T. Yu, Tau in neurodegenerative disease, Ann. Transl. Med. 6 (2018) 175.

[7] Y. Wang, E. Mandelkow, Tau in physiology and pathology, Nat. Rev. Neurosci. 17 (2016) 5–21.

[8] M. von Bergen, S. Barghorn, J. Biernat, E.M. Mandelkow, E. Mandelkow, Tau aggregation is driven by a transition from random coil to beta sheet structure, BBA 1739 (2005) 158–166.

[9] V. Daebel, S. Chinnathambi, J. Biernat, M. Schwalbe, B. Habenstein, A. Loquet, E. Akoury, K. Tepper, H. Muller, M. Baldus, C. Griesinger, M. Zweckstetter, E. Mandelkow, V. Vijayan, A. Lange, beta-Sheet core of tau paired helical filaments revealed by solid-state NMR, J. Am. Chem. Soc. 134 (2012) 13982–13989.

[10] J. Avila, J.J. Lucas, M. Perez, F. Hernandez, Role of tau protein in both physiological and pathological conditions, Physiol. Rev. 84 (2004) 361–384.

[11] B. Bader, G. Nubling, A. Mehle, S. Nobile, H. Kretzschmar, A. Giese, Single particle analysis of tau oligomer formation induced by metal ions and organic solvents, Biochem. Biophys. Res. Commun. 411 (2011) 190–196.

[12] G. Nubling, B. Bader, J. Levin, J. Hildebrandt, H. Kretzschmar, A. Giese, Synergistic influence of phosphorylation and metal ions on tau oligomer formation and coaggregation with alpha-synuclein at the single molecule level, Mol. Neurodegener. 7 (2012) 35.

[13] N. Kfoury, B.B. Holmes, H. Jiang, D.M. Holtzman, M.I. Diamond, Trans-cellular propagation of Tau aggregation by fibrillar species, J. Biol. Chem. 287 (2012) 19440–19451.

[14] J.L. Guo, V.M. Lee, Neurofibrillary tangle-like tau pathology induced by synthetic tau fibrils in primary neurons over-expressing mutant tau, FEBS Lett. 587 (2013) 717–723.

[15] K. Flach, I. Hilbrich, A. Schiffmann, U. Gartner, M. Kruger, M. Leonhardt, H. Waschipky, L. Wick, T. Arendt, M. Holzer, Tau oligomers impair artificial membrane integrity and cellular viability, J. Biol. Chem. 287 (2012) 43223–43233.

[16] C.A. Lasagna-Reeves, D.L. Castillo-Carranza, U. Sengupta, J. Sarmiento, J. Troncoso, G.R. Jackson, R. Kayed, Identification of oligomers at early stages of tau aggregation in Alzheimer's disease, FASEB J. 26 (2012) 1946–1959.

[17] C. Cardenas-Aguayo Mdel, L. Gomez-Virgilio, S. DeRosa, M.A. Meraz-Rios, The role of tau oligomers in the onset of Alzheimer's disease neuropathology, ACS Chem. Neurosci. 5 (2014) 1178–1191.

[18] M.A. Busche, S. Wegmann, S. Dujardin, C. Commins, J. Schiantarelli, N. Klickstein, T.V. Kamath, G.A. Carlson, I. Nelken, B.T. Hyman, Tau impairs neural circuits, dominating amyloid-beta effects, in Alzheimer models in vivo, Nat. Neurosci. 22 (2019) 57–64.

[19] C.M. Cowan, A. Mudher, Are tau aggregates toxic or protective in tauopathies? Front. Neurol. 4 (2013) 114.

[20] C.A. Lasagna-Reeves, D.L. Castillo-Carranza, U. Sengupta, A.L. Clos, G.R. Jackson, R. Kayed, Tau oligomers impair memory and induce synaptic and mitochondrial dysfunction in wild-type mice, Mol. Neurodegener. 6 (2011) 39.

[21] D.L. Castillo-Carranza, M.J. Guerrero-Munoz, U. Sengupta, C. Hernandez, A.D. Barrett, K. Dineley, R. Kayed, Tau immunotherapy modulates both pathological tau and upstream amyloid pathology in an Alzheimer's disease mouse model, J. Neurosci. 35 (2015) 4857–4868.

[22] K.R. Patterson, C. Remmers, Y. Fu, S. Brooker, N.M. Kanaan, L. Vana, S. Ward, J.F. Reyes, K. Philibert, M.J. Glucksman, L.I. Binder, Characterization of prefibrillar Tau oligomers in vitro and in Alzheimer disease, J. Biol. Chem. 286 (2011) 23063–23076.

[23] E.R. Georgieva, S. Xiao, P.P. Borbat, J.H. Freed, D. Eliezer, Tau binds to lipid membrane surfaces via short amphipathic helices located in its microtubule-binding repeats, Biophys. J. 107 (2014) 1441–1452.

[24] C.N. Chirita, M. Necula, J. Kuret, Anionic micelles and vesicles induce tau fibrillization in vitro, J. Biol. Chem. 278 (2003) 25644–25650.

[25] S. Elbaum-Garfinkle, T. Ramlall, E. Rhoades, The role of the lipid bilayer in tau aggregation, Biophys. J. 98 (2010) 2722–2730.

[26] E.M. Jones, M. Dubey, P.J. Camp, B.C. Vernon, J. Biernat, E. Mandelkow, J. Majewski, E.Y. Chi, Interaction of tau protein with model lipid membranes induces tau structural compaction and membrane disruption, Biochemistry 51 (2012) 2539–2550.

[27] C.A. Lasagna-Reeves, U. Sengupta, D. Castillo-Carranza, J.E. Gerson, M. Guerrero-Munoz, J.C. Troncoso, G.R. Jackson, R. Kayed, The formation of tau pore-like structures is prevalent and cell specific: possible implications for the disease phenotypes, Acta Neuropathol. Commun. 2 (2014) 56.

[28] J.A. Amorim, P.M. Canas, A.R. Tome, A.P. Rolo, P. Agostinho, C.M. Palmeira, R.A. Cunha, Mitochondria in excitatory and inhibitory synapses have similar susceptibility to amyloid-beta peptides modeling Alzheimer's disease, J. Alzheimers Dis. 60 (2017) 525–536.

[29] Z. Berger, H. Roder, A. Hanna, A. Carlson, V. Rangachari, M. Yue, Z. Wszolek, K. Ashe, J. Knight, D. Dickson, C. Andorfer, T.L. Rosenberry, J. Lewis, M. Hutton, C. Janus, Accumulation of pathological tau species and memory loss in a conditional model of tauopathy, J. Neurosci. 27 (2007) 3650–3662.

[30] D.C. David, S. Hauptmann, I. Scherping, K. Schuessel, U. Keil, P. Rizzu, R. Ravid, S. Drose, U. Brandt, W.E. Muller, A. Eckert, I. Gotz, Proteomic and functional analyses reveal a mitochondrial dysfunction in P301L tau transgenic mice, J. Biol. Chem. 280 (2005) 23802–23814.

[31] B. DuBoff, J. Gotz, M.B. Feany, Tau promotes neurodegeneration via DRP1 mislocalization in vivo, Neuron 75 (2012) 618–632.

[32] R.A. Quintanilla, P.J. Dolan, Y.N. Jin, G.V. Johnson, Truncated tau and Abeta cooperatively impair mitochondria in primary neurons, Neurobiol. Aging 33 (619) (2012) e625–635.

[33] M.J. Perez, K. Vergara-Pulgar, C. Jara, F. Cabezas-Opazo, R.A. Quintanilla, Caspase-cleaved tau impairs mitochondrial dynamics in Alzheimer's disease, Mol. Neurobiol. 55 (2018) 1004–1018.

[34] D. Ardail, J.P. Privat, M. Egret-Charlier, C. Levrat, F. Lerme, P. Louisot, Mitochondrial contact sites.Lipid composition and dynamics, J. Biol. Chem. 265 (1990) 18797–18802.

[35] G. Paradies, V. Paradies, V. De Benedictis, F.M. Ruggiero, G. Petrosillo, Functional role of cardiolipin in mitochondrial bioenergetics, BBA 2014 (1837) 408–417.

[36] K. Suga, A. Hamasaki, J. Chinzaka, H. Umakoshi, Liposomes modified with cardiolipin can act as a platform to regulate the potential flux of NADP(+)-dependent isocitrate dehydrogenase, Metab. Eng. Commun. 3 (2016) 8–14.

[37] V.E. Kagan, V.A. Tyurin, J. Jiang, Y.Y. Tyurina, V.B. Ritov, A.A. Amoscato, A.N. Osipov, N.A. Belikova, A.A. Kapralov, V. Kini, I.I. Vlasova, Q. Zhao, M. Zou, P. Di, D.A. Svistunenko, I.V. Kurnikov, G.G. Borisenko, Cytochrome c acts as a cardiolipin oxygenase required for release of proapoptotic factors, Nat. Chem. Biol. 1 (2005) 223–232.

[38] Z.T. Schug, E. Gottlieb, Cardiolipin acts as a mitochondrial signalling platform to launch apoptosis, BBA 1788 (2009) 2022–2031.

[39] A. Camilleri, C. Zarb, M. Caruana, U. Ostermeier, S. Ghio, T. Hogen, F. Schmidt, A. Giese, N. Vassallo, Mitochondrial membrane permeabilisation by amyloid aggregates and protection by polyphenols, BBA 2013 (1828) 2532–2543.

[40] J. Wagner, S. Krauss, S. Shi, S. Ryazanov, J. Steffen, C. Miklitz, A. Leonov, A. Kleinknecht, B. Goricke, J.H. Weishaupt, D. Weckbecker, A.M. Reiner, W. Zinth, J. Levin, D. Ehninger, S. Remy, H.A. Kretzschmar, C. Griesinger, A. Giese, M. Fuhrmann, Reducing tau aggregates with anle138b delays disease progression in a mouse model of tauopathies, Acta Neuropathol. 130 (2015) 619–631.

[41] J.M. Petit, A. Maftah, M.H. Ratinaud, R. Julien, 10N-nonyl acridine orange interacts with cardiolipin and allows the quantification of this phospholipid in isolated mitochondria, Eur. J. Biochem. 209 (1992) 267–273.

[42] V. Kruger, M. Deckers, M. Hildenbeutel, M. van der Laan, M. Hellmers, C. Dreker, M. Preuss, J.M. Herrmann, P. Rehling, R. Wagner, M. Meinecke, The mitochondrial oxidase assembly protein1 (Oxa1) insertase forms a membrane pore in lipid bilayers, J. Biol. Chem. 287 (2012) 33314–33326.

[43] C.T. Chu, J. Ji, R.K. Dagda, J.F. Jiang, Y.Y. Tyurina, A.A. Kapralov, V.A. Tyurin, N. Yanamala, I.H. Shrivastava, D. Mohammadyani, K.Z.Q. Wang, J. Zhu, J. Klein-Seetharaman, K. Balasubramanian, A.A. Amoscato, G. Borisenko, Z. Huang, A.M. Gusdon, A. Cheikhi, E.K. Steer, R. Wang, C. Baty, S. Watkins, I. Bahar, H. Bayir, V.E. Kagan, Cardiolipin externalization to the outer mitochondrial membrane acts as an elimination signal for mitophagy in neuronal cells, Nat. Cell Biol. 15 (2013) 1197–1205.

[44] F. Schmidt, J. Levin, F. Kamp, H. Kretzschmar, A. Giese, K. Botzel, Single-channel

electrophysiology reveals a distinct and uniform pore complex formed by alpha-synuclein oligomers in lipid membranes, PLoS ONE 7 (2012) e42545.

[45] T. Gutsmann, T. Heimburg, U. Keyser, K.R. Mahendran, M. Winterhalter, Protein reconstitution into freestanding planar lipid membranes for electrophysiological characterization, Nat. Protoc. 10 (2015) 188–198.

[46] L. Tosatto, A.O. Andrighetti, N. Plotegher, V. Antonini, I. Tessari, L. Ricci, L. Bubacco, M. Dalla Serra, Alpha-synuclein pore forming activity upon membrane association, BBA 1818 (2012) 2876–2883.

[47] G. Perkins, C. Renken, M.E. Martone, S.J. Young, M. Ellisman, T. Frey, Electron tomography of neuronal mitochondria: three-dimensional structure and organization of cristae and membrane contacts, J. Struct. Biol. 119 (1997) 260–272.

[48] T. Kobayashi, S. Kuroda, M. Tada, K. Houkin, Y. Iwasaki, H. Abe, Calcium-induced mitochondrial swelling and cytochrome c release in the brain: its biochemical characteristics and implication in ischemic neuronal injury, Brain Res. 960 (2003) 62–70.

[49] P.X. Petit, M. Goubern, P. Diolez, S.A. Susin, N. Zamzami, G. Kroemer, Disruption of the outer mitochondrial membrane as a result of large amplitude swelling: the impact of irreversible permeability transition, FEBS Lett. 426 (1998) 111–116.

[50] B. O'Rourke, Mitochondrial ion channels, Annu. Rev. Physiol. 69 (2007) 19–49.

[51] P. Bernardi, The mitochondrial permeability transition pore: a mystery solved? Front. Physiol. 4 (2013) 95.

[52] G.X. Zhang, S. Kimura, K. Murao, K. Obata, H. Matsuyoshi, M. Takaki, Inhibition of cytochrome c release by 10-N-nonyl acridine orange, a cardiolipin-specific dye, during myocardial ischemia-reperfusion in the rat, Am. J. Physiol. Heart Circ. Physiol. 298 (2010) H433–439.

[53] A. Maftah, J.M. Petit, R. Julien, Specific interaction of the new fluorescent dye 10-N-nonyl acridine orange with inner mitochondrial membrane.A lipid-mediated inhibition of oxidative phosphorylation, FEBS Lett. 260 (1990) 236–240.

[54] T. Ichimura, M. Ito, K. Takahashi, K. Oyama, K. Sakurai, Involvement of mitochondrial swelling in cytochrome *c* release from mitochondria treated with calcium and Alloxan, J. Biophys. Chem. 2 (2011) 10–18.

[55] A. Godard, D. Heymann, S. Raher, I. Anegon, M.A. Peyrat, B. Le Mauff, E. Mouray, M. Gregoire, K. Virdee, J.P. Soulillou, et al., High and low affinity receptors for human interleukin for DA cells/leukemia inhibitory factor on human cells.Molecular characterization and cellular distribution, J. Biol. Chem. 267 (1992) 3214–3222.

[56] S. Takamori, M. Holt, K. Stenius, E.A. Lemke, M. Gronborg, D. Riedel, H. Urlaub, S. Schenck, B. Brugger, P. Ringler, S.A. Muller, B. Rammner, F. Grater, J.S. Hub, B.L. De Groot, G. Mieskes, Y. Moriyama, J. Klingauf, H. Grubmuller, J. Heuser, F. Wieland, R. Jahn, Molecular anatomy of a trafficking organelle, Cell 127 (2006) 831–846.

[57] V. Rhein, X. Song, A. Wiesner, L.M. Ittner, G. Baysang, F. Meier, L. Ozmen, H. Bluethmann, S. Drose, U. Brandt, E. Savaskan, C. Czech, J. Gotz, A. Eckert, Amyloid-beta and tau synergistically impair the oxidative phosphorylation system in triple transgenic Alzheimer's disease mice, Proc. Natl. Acad. Sci. U S A 106 (2009) 20057–20062.

[58] Y. Hu, X.C. Li, Z.H. Wang, Y. Luo, X. Zhang, X.P. Liu, Q. Feng, Q. Wang, Z. Yue, Z. Chen, K. Ye, J.Z. Wang, G.P. Liu, Tau accumulation impairs mitophagy via increasing mitochondrial membrane potential and reducing mitochondrial Parkin, Oncotarget 7 (2016) 17356–17368.

[59] T. Wieprecht, M. Beyermann, J. Seelig, Binding of antibacterial magainin peptides to electrically neutral membranes: thermodynamics and structure, Biochemistry 38 (1999) 10377–10387.

[60] J.A. Hebda, A.D. Miranker, The interplay of catalysis and toxicity by amyloid intermediates on lipid bilayers: insights from type II diabetes, Annu. Rev. Biophys. 38 (2009) 125–152.

[61] H.W. Huang, F.Y. Chen, M.T. Lee, Molecular mechanism of Peptide-induced pores in membranes, Phys. Rev. Lett. 92 (2004) 198304.

[62] A. Quist, I. Doudevski, H. Lin, R. Azimov, D. Ng, B. Frangione, B. Kagan, J. Ghiso, R. Lal, Amyloid ion channels: a common structural link for protein-misfolding disease, Proc. Natl. Acad. Sci. U S A 102 (2005) 10427–10432.

[63] B.L. Kagan, Membrane pores in the pathogenesis of neurodegenerative disease, Prog. Mol. Biol. Transl. Sci. 107 (2012) 295–325.

[64] D.C. Bode, M.D. Baker, J.H. Viles, Ion channel formation by amyloid-beta42 oligomers but not amyloid-beta40 in cellular membranes, J. Biol. Chem. 292 (2017) 1404–1413.

[65] N. Patel, S. Ramachandran, R. Azimov, B.L. Kagan, R. Lal, Ion channel formation by tau protein: implications for Alzheimer's disease and tauopathies, Biochemistry 54 (2015) 7320–7325.

[66] M.I. Garcia Fernandez, D. Ceccarelli, U. Muscatello, Use of the fluorescent dye 10-N-nonyl acridine orange in quantitative and location assays of cardiolipin: a study on different experimental models, Anal. Biochem. 328 (2004) 174–180.

[67] E. Mileykovskaya, W. Dowhan, R.L. Birke, D. Zheng, L. Lutterodt, T.H. Haines, Cardiolipin binds nonyl acridine orange by aggregating the dye at exposed hydrophobic domains on bilayer surfaces, FEBS Lett. 507 (2001) 187–190.

[68] P. Kaewsuya, N.D. Danielson, D. Ekhterae, Fluorescent determination of cardiolipin using 10-N-nonyl acridine orange, Anal. Bioanal. Chem. 387 (2007) 2775–2782.

[69] S.S. Dicke, L. Tatge, P.E. Engen, M. Culp, L.R. Masterson, Isothermal titration calorimetry and vesicle leakage assays highlight the differential behaviors of tau

[70] repeat segments upon interaction with anionic lipid membranes, Biochem. Biophys. Res. Commun. 493 (2017) 1504–1509.

[70] A. Martinez Hernandez, H. Urbanke, A.L. Gillman, J. Lee, S. Ryazanov, H.Y. Agbemenyah, E. Benito, G. Jain, L. Kaurani, G. Grigorian, A. Leonov, N. Rezaei-Ghaleh, P. Wilken, F.T. Arce, J. Wagner, M. Fuhrmann, M. Caruana, A. Camilleri, N. Vassallo, M. Zweckstetter, R. Benz, A. Giese, A. Schneider, M. Korte, R. Lal, C. Griesinger, G. Eichele, A. Fischer, The diphenylpyrazole compound anle138b blocks Abeta channels and rescues disease phenotypes in a mouse model for amyloid pathology, EMBO Mol. Med. 10 (2018) 32–47.

[71] R.N. Lewis, R.N. McElhaney, The physicochemical properties of cardiolipin bilayers and cardiolipin-containing lipid membranes, BBA 1788 (2009) 2069–2079.

[72] J.D. Unsay, K. Cosentino, Y. Subburaj, A.J. Garcia-Saez, Cardiolipin effects on membrane structure and dynamics, Langmuir 29 (2013) 15878–15887.

[73] T.N. Zeczycki, J. Whelan, W.T. Hayden, D.A. Brown, S.R. Shaikh, Increasing levels of cardiolipin differentially influence packing of phospholipids found in the mitochondrial inner membrane, Biochem. Biophys. Res. Commun. 450 (2014) 366–371.

[74] C. Giannattasio, G. Seravalle, G.B. Bolla, B.M. Cattaneo, J. Cleroux, C. Cuspidi, L. Sampieri, G. Grassi, G. Mancia, Cardiopulmonary receptor reflexes in normotensive athletes with cardiac hypertrophy, Circulation 82 (1990) 1222–1229.

[75] E.R. Pennington, E.M. Sullivan, A. Fix, S. Dadoo, T.N. Zeczycki, A. DeSantis, U. Schlattner, R.A. Coleman, A.J. Chicco, D.A. Brown, S.R. Shaikh, Proteolipid domains form in biomimetic and cardiac mitochondrial vesicles and are regulated by cardiolipin concentration but not monolyso-cardiolipin, J. Biol. Chem. 293 (2018) 15933–15946.

[76] E. Mileykovskaya, W. Dowhan, Cardiolipin-dependent formation of mitochondrial respiratory supercomplexes, Chem. Phys. Lipids 179 (2014) 42–48.

[77] R.F. Epand, M. Tokarska-Schlattner, U. Schlattner, T. Wallimann, R.M. Epand, Cardiolipin clusters and membrane domain formation induced by mitochondrial proteins, J. Mol. Biol. 365 (2007) 968–980.

[78] S.M. Claypool, Y. Oktay, P. Boontheung, J.A. Loo, C.M. Koehler, Cardiolipin defines the interactome of the major ADP/ATP carrier protein of the mitochondrial inner membrane, J. Cell Biol. 182 (2008) 937–950.

[79] G. Amadoro, V. Corsetti, A. Stringaro, M. Colone, S. D'Aguanno, G. Meli, M. Ciotti, G. Sancesario, A. Cattaneo, R. Bussani, D. Mercanti, P. Calissano, A NH2 tau fragment targets neuronal mitochondria at AD synapses: possible implications for neurodegeneration, J. Alzheimers Dis. 21 (2010) 445–470.

[80] D. Cieri, M. Vicario, F. Vallese, B. D'Orsi, P. Berto, A. Grinzato, C. Catoni, D. De Stefani, R. Rizzuto, M. Brini, T. Cali, Tau localises within mitochondrial sub-compartments and its caspase cleavage affects ER-mitochondria interactions and cellular Ca(2+) handling, Biochim. Biophys. Acta, Mol. Basis Dis. 2018 (1864) 3247–3256.

[81] L. Luo, J. Yang, D. Liu, Integration and oligomerization of Bax protein in lipid bilayers characterized by single molecule fluorescence study, J. Biol. Chem. 289 (2014) 31708–31718.

[82] O. Landeta, A. Landajuela, A. Garcia-Saez, G. Basanez, Minimalist model systems reveal similarities and differences between membrane interaction modes of MCL1 and BAK, J. Biol. Chem. 290 (2015) 17004–17019.

[83] M. Lutter, M. Fang, X. Luo, M. Nishijima, X. Xie, X. Wang, Cardiolipin provides specificity for targeting of tBid to mitochondria, Nat. Cell Biol. 2 (2000) 754–761.

[84] F. Gonzalvez, F. Pariselli, O. Jalmar, P. Dupaigne, F. Sureau, M. Dellinger, E.A. Hendrickson, S. Bernard, P.X. Petit, Mechanistic issues of the interaction of the hairpin-forming domain of tBid with mitochondrial cardiolipin, PLoS ONE 5 (2010) e9342.

[85] T.H. Kim, Y. Zhao, W.X. Ding, J.N. Shin, X. He, Y.W. Seo, J. Chen, H. Rabinowich, A.A. Amoscato, X.M. Yin, Bid-cardiolipin interaction at mitochondrial contact site contributes to mitochondrial cristae reorganization and cytochrome C release, Mol. Biol. Cell 15 (2004) 3061–3072.

[86] J. Jacobson, M.R. Duchen, S.J. Heales, Intracellular distribution of the fluorescent dye nonyl acridine orange responds to the mitochondrial membrane potential: implications for assays of cardiolipin and mitochondrial mass, J. Neurochem. 82 (2002) 224–233.

[87] C.W. Leung, Y. Hong, J. Hanske, E. Zhao, S. Chen, E.V. Pletneva, B.Z. Tang, Superior fluorescent probe for detection of cardiolipin, Anal. Chem. 86 (2014) 1263–1268.

[88] R.M. Epand, C. Walker, R.F. Epand, N.A. Magarvey, Molecular mechanisms of membrane targeting antibiotics, BBA 2016 (1858) 980–987.

[89] L. Yang, V.D. Gordon, D.R. Trinkle, N.W. Schmidt, M.A. Davis, C. DeVries, A. Som, J.E. Cronan Jr., G.N. Tew, G.C. Wong, Mechanism of a prototypical synthetic membrane-active antimicrobial: efficient hole-punching via interaction with negative intrinsic curvature lipids, Proc. Natl. Acad. Sci. U S A 105 (2008) 20595–20600.

[90] K. Scheinpflug, O. Krylova, H. Nikolenko, C. Thurm, M. Dathe, Evidence for a novel mechanism of antimicrobial action of a cyclic R-, W-rich hexapeptide, PLoS One 10 (2015) e0125056.

[91] A.V. Birk, S. Liu, Y. Soong, W. Mills, P. Singh, J.D. Warren, S.V. Seshan, J.D. Pardee, H.H. Szeto, The mitochondrial-targeted compound SS-31 re-energizes ischemic mitochondria by interacting with cardiolipin, J. Am. Soc. Nephrol. 24 (2013) 1250–1261.

[92] H.H. Szeto, First-in-class cardiolipin-protective compound as a therapeutic agent to restore mitochondrial bioenergetics, Br. J. Pharmacol. 171 (2014) 2029–2050.